View Article Online
View Journal

Environmental Science Nano

Accepted Manuscript

This article can be cited before page numbers have been issued, to do this please use: M. R. Hamode, A. Krause, M. shehadeh, T. Zar, B. schmerling, I. Pinkas, D. Zitoun and A. Salomon, *Environ. Sci.: Nano*, 2024, DOI: 10.1039/D3EN00821E.

ROYAL SOCIETY OF CHEMISTRY

rsc.li/es-nano

View Article Online
DOI: 10.1039/D3EN00821E

ARTICLE

Plasmonic Based Raman sensor for Ultra-sensitive detection of Pharmaceutical waste

Mohamed Hamode, [ab] Alon Krause [ab], Maria Shehadeh[ab], Bruria Schmerling [a], Tchiya Zar [ab], Iddo Pinkas [c], David Zitoun [ab], and Adi Salomon*[ab]

Received 00th January 20xx,
Accepted 00th January 20xx

DOI: 10.1039/x0xx00000x

Pharmaceutical waste and contaminants pose a significant global concern for water and food safety. The detection of piperidine, a common residue in drug and supplement synthesis, is critical due to its toxic nature to both humans and animals. In this study, we develop a plasmonic-based detector for surface enhanced Raman scattering (SERS) measurements. The plasmonic device is composed of triangular cavities, milled in silver thin film and protected by 5 nm of SiO_2 layer. Due to the confined and enhanced electromagnetic field, remarkable sensitivity to piperidine with concentration of 10^{-8}M in water is achieved. Despite the relative small polarizability of piperidine, high sensitivity is observed even when using a low numerical aperture of 0.3., attributing to the directional scattring from our plasmonic device. Thus, It offers a cost-effective alternative to traditional high numerical aperture used in SERS, and the ability to use a portable Raman device for a cheaper and faster analysis.

Environmental significance

Piperidine is a small potent molecule that serves as a crucial building block in the pharmaceutical and food additive industries, although it is toxic in nature. Unfortunately, it can also be found in drinking water as a result of pharmaceutical waste. Therefore, development of an optical-sensitive detector is crucial for the environment. Raman scattering is a sensitive optical technique; but its contribution to environmental monitoring is negligible. Moreover, the required optics for Raman scattering are often demanding and expensive, making the instrument challenging to use in environmental science. Using our nano-patterned metallic surfaces, the detection of low concentrations of piperidine in water using affordable optics is possible. The utilization of these surfaces presents an opportunity to employ portable cost-effective Raman devices as environmental analytical set-up.

1. Introduction

In spontaneous Raman scattering, the Raman effect is remarkably feeble, typically resulting in only 1 out of 10^8 incident radiation events undergoes spontaneous Raman scattering [1–4]. Employing lasers with relatively high power and objectives featuring a high numerical aperture (N.A.) allow for the collection of sufficient scattered photons. Yet, such a set-up is expensive and inadequate for many practical applications. Thus, finding solutions to enhance the Raman responses are always necessary. Metallic nano-structures may lead to deep sub-wavelength confinement and amplification of the Electromagnetic (EM) field due to excitation of plasmonic modes[5,6]. This can yield remarkably strong SERS responses, often spanning over several orders of magnitude. Therefore, it is not surprising that over the past decade, SERS has emerged as a potent analytical technique, renowned for its ability to detect trace amounts of chemicals with exceptional sensitivity and specificity[7–10]. Applications of SERS were realized in various fields, encompassing environmental science, biology, food safety, medicine, chemistry, and more. Notably, SERS has been

[a] Department of Chemistry, Bar-Ilan University, Ramat-Gan 5290002, Israel.
[b] Institute of Nanotechnology and Advanced Materials (BINA), Bar-Ilan University, Ramat-Gan 5290002, Israel.
[c] Department of Chemical Research Support, Weizmann Institute of Science, Rehovot, Israel
[d] * E-mail: Adi.Salomon@biu.ac.il http://orcid.org/0000-0002-5643-0478
[e] † Cross-section and surface morphology analysis, Transmission spectra of the arrays, Vibrational modes of the piperidine molecule, Comparison between Raman spectra of the SERS device (p400 nm), non-well milled arrays: surface morphology and low sensitivity. See DOI: 10.1039/x0xx00000x

View Article Online
DOI: 10.1039/D3EN00824E

instrumental in the field of COVID-19 diagnostics[11], specifically in the identification of the SARS-CoV-2 virus within nasal swab samples, achieving an impressive accuracy of about 250 fg/mL [12–16].

Within the realm of environmental science[17], SERS has been effectively employed for the monitoring of heavy metal levels and the detection of microplastics in water[18,19]. Moreover, SERS has proven effective in detecting and quantifying pesticides[20–26], food additives[27–29], drug residues[30,31], and industrial discharges[32,33] within food and water samples. In the field of biology, SERS has facilitated high-resolution imaging of cells and tissues, offering detailed insights into their chemical composition, which holds a potential for diagnosing various diseases[34,35]. Furthermore, SERS has shown promising results in drug delivery applications, allowing for the monitoring of drug release from nanoparticles and providing valuable kinetic information regarding the process[36–40].

Despite the advances in SERS over the last few decades, several challenges still persist. These include the reliable detection of small molecules, the durability of SERS substrates, signal stability, and the use of cost-effective optics.

Herein, we use plasmonic cavities milled in a thin silver film and protected by a thin silica layer to enhance the Raman signal. With our developed plasmonic surfaces, low concentrations of 10^{-8}M of piperidine in water can be detected. Furthermore, due to directed scattering of the Raman signal from the plasmonic surfaces, enhanced signal can be measured, using a low N.A. of 0.3. Furthermore, we show that a mix of analytes can be distinguished as well, by using our SERS substrate.

We undertook the challenge of detection of the small molecule piperidine because this molecule and its derivatives play a pivotal role as fundamental building blocks in the pharmaceutical industry for the synthesis of drugs and supplements. More than 70 FDA-approved drugs contain the piperidine moiety [4142]. Piperidine can be found as a derivative in various pharmaceuticals, including selective estrogen receptor modulators (SERMs) like minoxidil, opioids, antipsychotic drugs such as Melperone, and insect repellent products. Another source of piperidine is the hydrolysis of piperine, a naturally occurring compound found in plants such as pepper[43]. Humans are exposed to piperidine on a daily basis, as evidenced by its wide presence in the food supply and, consequently, in human urine. As a food additive, piperidine is found at 2.5-3.33 ppm in nonalcoholic beverages, 4-5.67 ppm in candy, 9.69 ppm in baked goods, and 0.04-1.66 ppm in condiments, meats, and soups. Baked ham contains 0.2 ppm of piperidine, milk 0.11 ppm, and dry coffee 1 ppm[44]. Von Euler reported that humans excrete 7.6-8.5 mg of piperidine in a 24-h period[45]; more recently, Tricker et al reported excretion rates of 26.1-31.7 mg/day[46].

Figure 1a. shows the selected analyte, piperidine, and its derivatives from the different pharmaceutical drug families. This colorless molecule is known to be toxic to both humans and animals, even at low concentrations, with an LD50 value of 30 mg/kg. Inhalation of high vapor concentrations of piperidine may lead to symptoms such as weakness, dizziness, headache, nausea, vomiting, labored breathing, increased heart rate, and elevated blood pressure[47]. Additionally, piperidine is corrosive to the skin and eyes upon contact, and it can readily penetrate the skin, thereby being considered toxic through dermal exposure as well. Sensors for piperidine are mainly based on an electrochemical detection, for example: by using hollow mesoporous ZnO on carbon electrode, detection limit of ~3.3 µM was realized[48]. Additionally, a detection limit of ~60 nM was achieved with a direct grown of well-aligned ZnO nano-rods on conductive electrode substrate [49] . Yet, the durability of those electrodes is not high, as they can become contaminated over time leading to reduced sensitivity and accuracy. In addition, this technique has limited sensitivity when dealing with low concentrations. Our presented SERS substrates contain additional protective 5 nm thin layer of SiO_2 and therefore, they demonstrate high sensitivity, rapid analysis, low-cost preparation, and long-term stability. It allows for repeated use without significant degradation in performance. This is in contrast to some electrochemical electrodes, which may require frequent replacement or maintenance.

2. Materials and methods

2.1. Sample preparation

2.1.1. Substrate cleaning and metallic layer sputtering

To achieve high quality sliver films with low roughness, fused silica substrates (170 micrometer thickness) were dipped into a diluted aqueous solution of "Hellmanex III" cleaning solvent (1/100, v/v), followed by mild bath-sonication at 30 °C for 20 minutes. Afterwards, the substrates were washed thoroughly with di-ionized (DI) water (18.2 MΩ) and subsequently with ethanol. The substrates were dried by a continuous stream of nitrogen (99.999%). A thin silver layer (~200 nm) was deposited onto the clean substrates using a sputtering instrument (Quorum, Q150TS). To obtain smooth films, the Ar atoms were ionized by electric current (100 mA), with a vacuum pressure of 1×10^{-4} Torr. To verify the whole process, calibration measurements have been done by Focused Ion Beam (FIB), cross-section measurements (See Figure S1).

2.1.2. Fabrication of plasmonic structures

Plasmonic structures were milled by a focused ion beam (FIB), (Helios NanoLab DualBeam 600, FEI). The sub-units that comprise the nanostructures were isosceles triangular nanocavities with a typical side-length of 215 nm and a base length of 200 nm (see Fig. 1b and S1†). Before milling, several scripts have been programmed while considering the FIB parameters. Both cubical and hexagonal arrays of triangular cavities were fabricated, in which the periodicities were varied from 400 to 700 nm with a 50 nm delta (P=400, 450, 500, etc.). Furthermore, to validate the reproducibility of the nano plasmonic structures, the process was thereafter repeated at least three times and on several samples. Prior to the milling procedure, parameters such as the beam current and the

number of passes have been calibrated so to obtain high quality plasmonic structures, which is a crucial parameter. The currents and voltages used for milling range from 9.7 to 48 pA, and 30 kV, respectively.

2.1.3. Deposition of a Thin SiO_2 Layer for protection

A thin silica layer of ~5nm was deposited on top of the silver layer (see fig S2† for characterization of the SiO_2 layer). This is to assure three outcomes: Firstly, to extend the shelf life of the SERS substrate and to be able to re-use it, second, to prevent oxidation of the silver layer and lastly to further functionalize the substrates with silane linkers for future applications. This process was done by electron-beam evaporation (BesTec, Germany) at 2.4×10^{-5} mBar and a current of 1 mA.

2.1.4. Analyte preparation

Piperidine was dissolved by ethanol and DI water in different concentrations (10^{-3}M-10^{-8}M). Some of solution have been measured also by mass- spectra to assure the solubility of the analyte and its concentration. After that, the plasmonic SERS substrate was immersed for 1-2 minutes in the solution that contains the analyte. Finally, the samples were dried with N_2 prior the Raman measurements as is shown in the illustration.

2.1. Optical Imaging and Spectra

The transmission imaging and spectra of the plasmonic nano-cavities were acquired using a bright field mode in an inverted microscope setup (OLYMPUS IX83). The samples were illuminated by a non-polarized collimated light. The transmitted light was directed to a spectrograph (IsoPlane SCT 320, Princeton Instruments) and then detected by a high quantum efficiency charge coupled device (CCD) camera (PIXS1024b) using an objective X40 magnification (N.A of 0.6). The grating used for acquiring the spectra was 50 grooves/mm (density), and the blaze wavelength is 600 nm (Princeton Instruments). The spectra were always collected under the same conditions (40x and N.A. of 0.6). All acquired spectra were normalized to the reference glass spectrum taken using the same parameters. The images and spectra obtained, give us valuable information regarding the plasmonic modes and their interaction with light. The symmetry, shape, size, and geometry of the cavities will dictate their optical response and would be elaborated in the results and discussion section later in this proposal thesis.

2.2. Raman spectroscopy measurements

Raman spectra were measured using LabRAM Soleil (Horiba, France) set-up. We used a 532 nm laser source with a low laser power of 0.55 mW, to ensure the stability of the measurements. The Spectra have been acquired in a region of 400 cm^{-1} to 2000 cm^{-1} with a 600 gr/mm grating, confocal hole of 200 µm and 1.3 cm^{-1}/pixel spectral dispersion. The sample was placed under an optical microscope, with the following objectives: ×50 N.A. 0.6 and X10 N.A. 0.3 (Nikon). Only clean samples have been measured, that is, if aggregation of the analytes was observed by the optical microscope - it was not measured. We have repeated those measurements with many samples, and 3 different Raman systems, and different conditions.

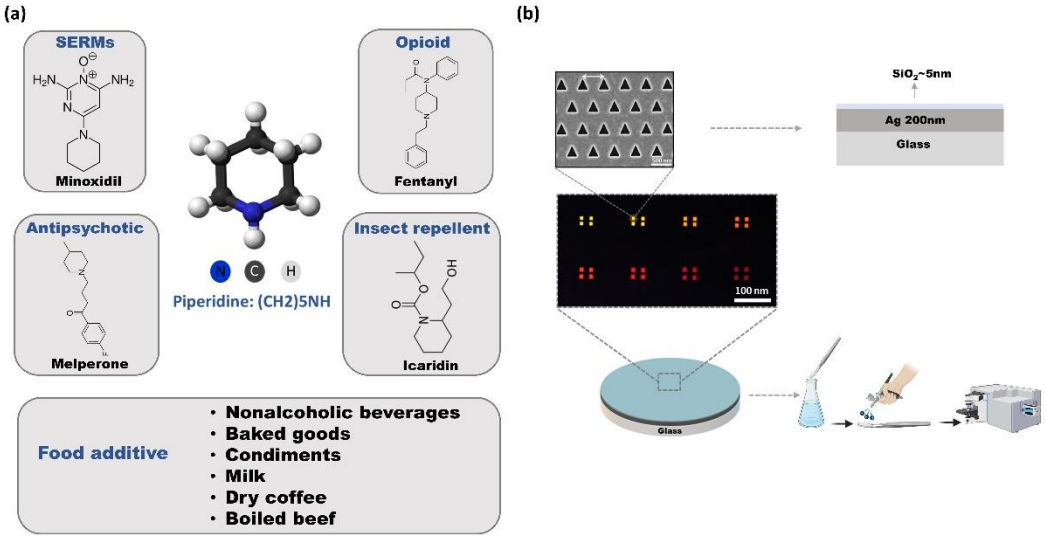

Fig. 1 (a) 3d chemical structure of piperidine, and its drug derivatives, food additive, explaining the reason for choosing this analyte. (b) our device, composed of a fused silica substrate covered by a smooth silver thin film (200 nm) and then covered with 5 nm of SiO2 for stability (see illustration of cross section). Series of hexagonal triangular hole-arrays were milled in the silver thin film, with different periodicities. SEM image of the plasmonic structure shows the accuracy of the FIB milling, and the uniformity of the structure. The light transmission color micrograph below is the transmission of light through a series of plasmonic structures (see also Figure S3 for the spectra). The fabricated plasmonic devices were immersed in different solutions and dried with N_2 as shown in the illustration.

3. Results and discussion

View Article Online
DOI: 10.1039/D3EN00821E

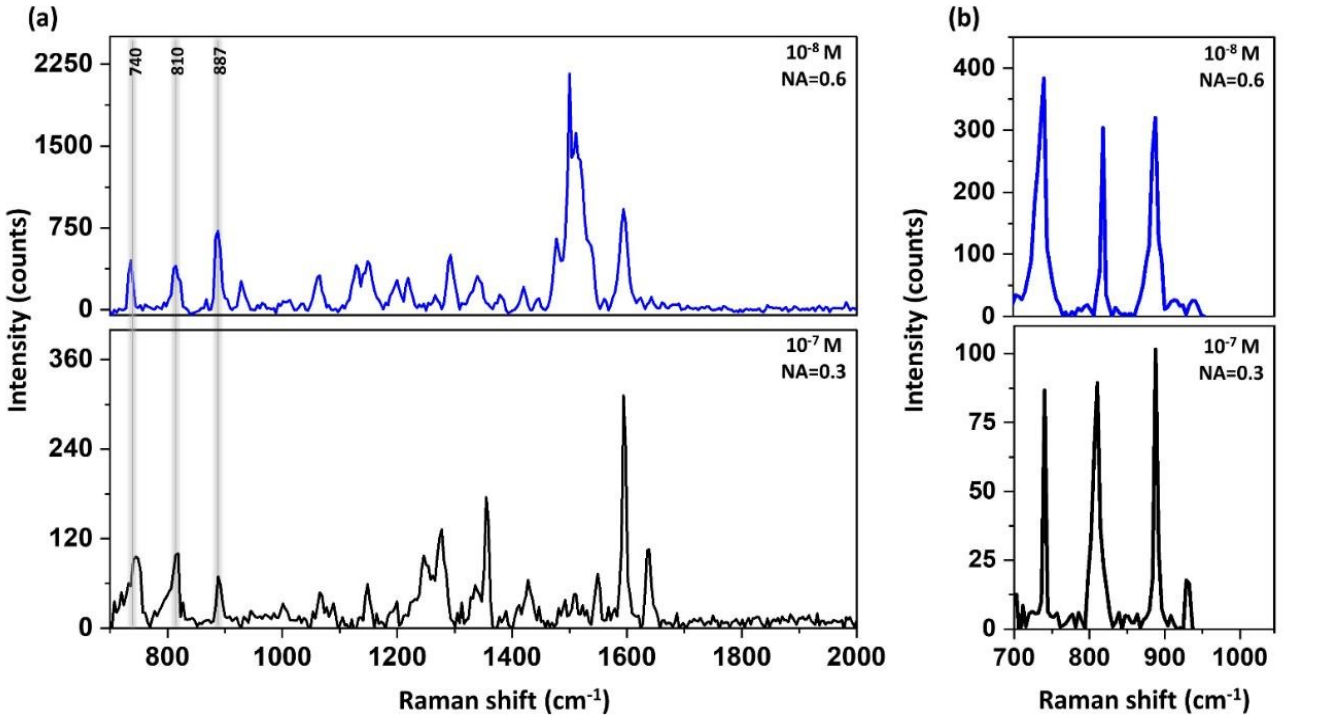

Fig. 2 Raman spectra taken from our plasmonic devices (hexagonal triangular array with periodicity of 400 nm after being immersed in solution of piperidine in ethanol (a) and then in DI water (b), with concentration of 10^{-8}M and 10^{-7}M, using N.A. of 0.6 and 0.3 respectively and laser power of 0.55mW.

Our plasmonic device is composed of hexagonal triangular nano-cavities with different periodicities, milled in 200 nm silver thin film and covered by 3-5 nm thin layer of SiO2 (see Fig. 1b). The observed different physical colors are due to extraordinary light transmission through the cavities at different wavelength (see Fig. S3† for the spectroscopic measurements). These unique plasmonic structures give rise to an enhanced Electromagnetic (EM) field at the vicinity of the surface, namely hot-spots, and deep sub-wavelength confinement of the EM field can be achieved. Therefore, nonlinear optical processes such as Raman can be boosted by orders of magnitudes. The array periodicity was tuned so to match the plasmonic mode resonance with the Raman laser wavelength as shown in Fig. S3†. Thus, herein we use a periodicity of about 400 nm, which has a considerable overlap between the plasmonic resonance and the wavelength of the laser (532 nm), as well as with scattered Raman photons at lower energy. The plasmonic device was carefully immersed in solutions containing piperidine at different concentrations and allowed to set for approximately two minutes. Following this, the device was gently removed from the solution, and dried by using a stream of nitrogen gas to remove any residual solvent. Finally, the sample was measured using a Raman system. It is worth noting that the plasmonic surface remains clean after this process, with no detectable aggregation of molecules, otherwise such samples were not measured.

Piperidine has a very small cross-section for Raman, nevertheless due to the enhanced EM field in proximity to the plasmonic structures, detection of this analyte by Raman is possible both in di-ionized (DI) water and in ethanol down to concentrations of 10^{-8}M, as is presented in Fig. 2. The blue spectra were taken using objective of N.A.=0.6, and the black spectra were taken using a lower N.A.= of 0.3. Yet, due to our plasmonic surfaces, which allow efficient directed scattering, we could measure the low concentration of 10^{-7}M of piperidine even using low N.A.= of 0.3 (see Fig 2). In essence, the plasmonic structure directs scattered emitted photons towards the detector, thereby requiring a reduced collection angle.

The enhancement factor was calculated to be $4 * 10^6$ as is shown in fig. S4†. Piperidine has several vibration modes[50] as is summarized in table S1† and Fig. S5†.

Herein, we focused on three characteristic peaks of piperidine: 740 cm^{-1}, 810 cm^{-1} and 887 cm^{-1} that assigned to: N-H deformation, ring "breathing" and C-N-C stretch, respectively[50]. The reason behind the focus on these peaks is due additional responses resulting from the ethanol solution alone and overlapping with the vibrational modes of piperidine above 1200 cm^{-1} (see Fig. S6†).

View Article Online
DOI: 10.1039/D3EN00821E

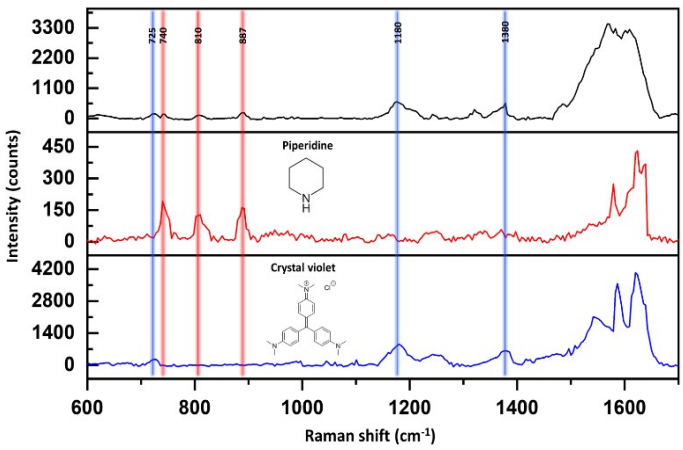

Fig. 3 Detection of mix analyte solution with concentration of 10^{-7}M in DI water using our plasmonic SERS substrate. The blue curve is SERS of CV, the red one is of piperidine, and the black one is for the mixture. The three SERS spectra were measured under the same conditions, with N.A.=0.6 (X50) objective and laser power of 0.55mW (532 nm) and acquisition time of 3s.

In addition, at the spectral regime above 1400 cm^{-1}, the signal was not stable and reproducible over time. The instability could stem from contamination on the silver surface, primarily caused by the introduction of carbon particles during the sputtering process. However, even though we have achieved highly clean surfaces, we believe it is valuable to have the capability to measure Raman responses of small molecules under realistic laboratory conditions. We argue that our SERS device in not only possess high sensitivity but also selectivity in water. Fig. 3 shows detection of 10^{-7}M crystal violet (CV), piperidine and they mixture (black curve) using our SERS substrate. The vibration modes of the CV that we focused on are: 725 cm^{-1} which is assigned to C-N-C stretching. The band at 1180 cm^{-1} is attributed to C–H in bending vibrations. The band at 1380 cm^{-1} is assigned to N-phenyl stretching. In the case of piperidine we focused on three characteristic peaks as discussed before. All those vibrations modes are presented in the Raman spectrum of their mixture. Yet, we are aware to the fact that other vibrational modes may be presented due to hydrogen bonds and re-organization of the analytes in the solutions, which can be a subject for future studies.

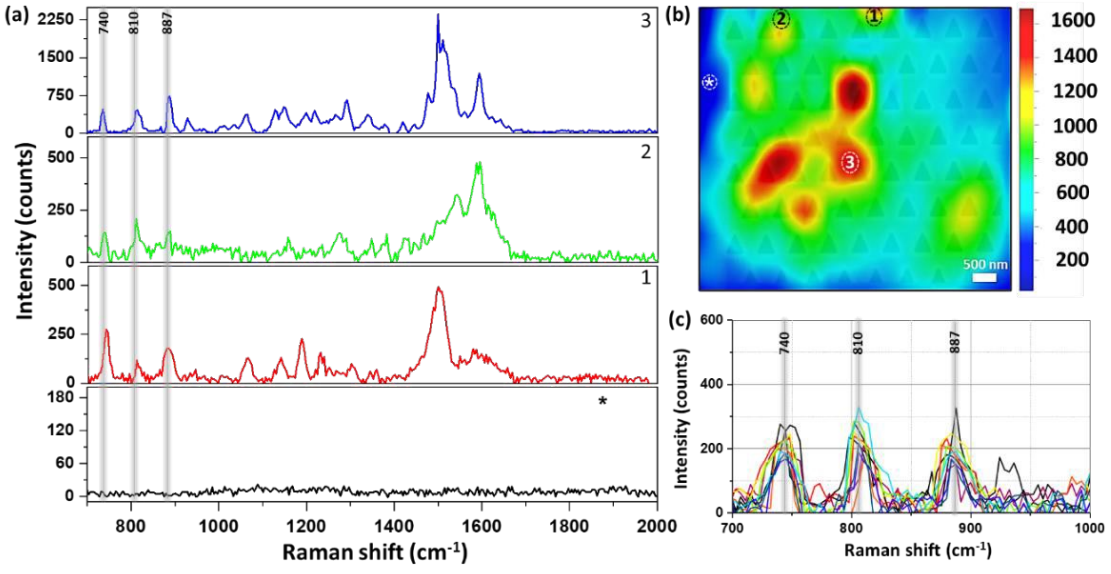

Fig. 4 (a) SERS spectra of 10^{-8}M piperidine in ethanol at different area onto the plasmonic surface, i.e., The black graph (*) was taken from the silver surface nearby the plasmonic structure. The three vibrational modes of piperidine (740, 810, 887 cm^{-1}), are marked for clarity. (b) Raman mapping of the plasmonic array. The spectral range of the map is 700 cm^{-1} -1000 cm^{-1}. And the numbers correspond to the area from which the spectra in (a) were taken. The SEM of the plasmonic stricture is fused for clarity (c) 10 SERS spectra of piperidine taken from multiple selected spots on the array. The experimental parameters are as follow: laser: λ=532 nm, power=0.55mW Objective of X50 magnification with N.A.=0.6, and acquisition time of 3s. The plasmonic structure is hexagonal triangular array (p=400nm).

View Article Online
DOI: 10.1039/D3EN00821E

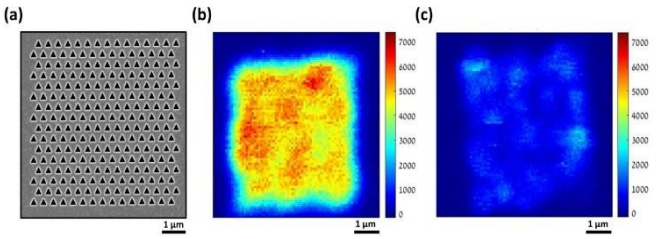

Fig. 5 Second Harmonic Generation (SHG) intensity maps of our plasmonic device. (a) a typical plasmonic array that was used in this study. (b) SHG scanning of (a), showing that the nonlinear responses are high, yet not uniform, in agreement with the Raman mapping. (c) an example of SHG mapping of plasmonic device in which the milling process was not good (see S5). Laser Power= 2mW, λω= 940 nm.

Figure 4 shows Raman mapping measurement of 10^{-8}M piperidine dissolved in ethanol using our plasmonic surfaces (p=400 nm) as is described above (see Fig. 1). Raman mapping was conducted both on the plasmonic array and on the smooth silver surface outside the array. It is noteworthy that negligible to nonexistent signals were detected on the smooth silver surface (Fig. 4a, black curve), even at higher concentrations, as no peaks were observed. However, within the array, clear spectra of piperidine were obtained, exhibiting the three vibration modes of interest (refer to spectra 1-3 and the corresponding map). The mapping presented in Fig. 4b reveals the nonhomogeneous responses of the array, with variations of up to threefold, indicating the presence of hot-spots where certain areas exhibit higher Raman responses compared to others. Importantly, we observe the presence of all three vibrational modes in different areas, validating the appropriateness of our selection. In addition, the reproducibly and the repetitively of those selected vibrational modes is notable in the 10 different spectra presented in Fig 4c (see also S7†;). If our fabricated plasmonic surfaces indeed possess hot-spots, which are characterized by localized regions of enhanced Raman responses, it is highly probable that these hot-spots will also be evident in the second harmonic generation (SHG) process, which is another nonlinear optical phenomenon. Hot-spots indicate areas with heightened local electromagnetic field intensities, thus significantly enhancing nonlinear optical processes like SHG. The hotspots depend on the unique atomic structure of the surface at the specific spot. Fig. 5 showcases the SHG scanning of the identical plasmonic structure with relatively low laser power of 2mW using N.A. of 0.5. The efficiency of this process heavily relies on the strength of the local electric field. The regions with the triangular cavities experience an intensified electric field enhancement, resulting in enhanced SHG signals compared to the surrounding areas. The nonlinear responses within the array exhibit notable variations, up to a factor of 3, while it is negligible outside the array on the flat silver surface. It is worth noting that inadequate fabrication or milling of the plasmonic array leads to a drastic suppression of the SHG response as shown in Fig. 5c (see also Fig. S8†). The coexistence of hot-spots in both Raman and SHG measurements suggests that enhanced local electromagnetic fields and nonlinear optical responses are present in the plasmonic structures, further affirming their potential for Raman sensing applications.

4. Conclusion

In conclusion, we have successfully demonstrated the detection piperidine both in water and ethanol solutions, down to a concentration of 10^{-8}M, utilizing a low numerical aperture N.A. of 0.3. This achievement was made possible by using our plasmonic array, which generates enhanced EM fields in the proximity of the array. Our SERS substrate is covered by 5nm of silica, increasing its stability and durability. In addition, a mixture of two analytes in water was successfully detected down to concertation of 10^{-7} M. The utilization of a low N.A. has an economic advantage as it eliminates the need to purchase a high numerical aperture system, thus reducing costs. Furthermore, the mapping image obtained from the Raman and SHG measurements confirms the presence of hot spots in the plasmonic array, validating its potential for enhancing signal intensities. For the specific detection of piperidine, we focused on the following peaks (740, 815, 887 cm^{-1}), as they remain unaffected by peak overlap resulting from the adsorption of common solvents and other contaminants commonly encountered on surfaces during experiments. This selection ensures reliable and accurate identification of piperidine in the presence of potential interfering factors.

Author Contributions

A.S and D.Z. supervised and designed this research. M.H. designed this research, fabricated samples, preformed measurements, and analysis. I.P, M.S. and B.R did together with M.H the Raman measurements. A.K did the SHG measurements. All authors contributed to the interpretation of data. M.H. and A.S. wrote the article.

Conflicts of interest

The authors assert they have no competing financial involvement.

References

1 L. A. Lyon, C. D. Keating, A. P. Fox, B. E. Baker, L. He, S. R. Nicew, S. P. Mulvaney and M. J. Natan, Raman Spectroscopy, 1998, **70**, 341–362.

2 P. Rostron, S. Gaber and D. Gaber, Raman Spectroscopy , a Review, *International Journal of Engineering and Technical Research (IJETR)*, 2016, **6**, 2454–4698.

3 A. Kudelski, Analytical applications of Raman spectroscopy, *Talanta*, 2008, **76**, 1–8.

4 R. S. Das and Y. K. Agrawal, Raman spectroscopy: Recent advancements, techniques and applications, *Vib Spectrosc*, 2011, **57**, 163–176.

5 X. Xue, Y. Fan, E. Segal, W. Wang, F. Yang, Y. Wang, F. Zhao, W. Fu, Y. Ling, A. Salomon and Z. Zhang, Periodical concentration of surface plasmon polaritons by wave interference in metallic film with nanocavity array, *Materials Today*, 2021, **46**, 54–61.

6 F. Zhao, W. Wang, H. Zhong, F. Yang, W. Fu, Y. Ling and Z. Zhang, Robust quantitative SERS analysis with Relative Raman scattering intensities, *Talanta*, DOI: 10.1016/j.talanta.2020.121465.

7 P. A. Mosier-Boss, Review of SERS substrates for chemical sensing, *Nanomaterials*, 2017, **7**, 142.

8 J. Perumal, Y. Wang, A. B. E. Attia, U. S. Dinish and M. Olivo, Towards a point-of-care SERS sensor for biomedical and agri-food analysis applications: A review of recent advancements, *Nanoscale*, 2021, **13**, 553–580.

9 B. Sharma, R. R. Frontiera, A. I. Henry, E. Ringe and R. P. Van Duyne, SERS: Materials, applications, and the future, *Materials Today*, 2012, **15**, 16–25.

10 C. Liu, D. Xu, X. Dong and Q. Huang, A review: Research progress of SERS-based sensors for agricultural applications, *Trends Food Sci Technol*, 2022, **128**, 90–101.

11 W. Wang, S. Kang, W. Zhou and P. J. Vikesland, *Environ Sci Nano*, 2022, 10, 393–423.

12 D. Antoine, M. Mohammadi, M. Vitt, J. M. Dickie, S. S. Jyoti, M. A. Tilbury, P. A. Johnson, K. E. Wawrousek and J. G. Wall, Rapid, Point-of-Care scFv-SERS Assay for Femtogram Level Detection of SARS-CoV-2, *ACS Sens*, 2022, **7**, 866–873.

13 A. A. Kowalska, SERS Signature of SARS-CoV-2 in Saliva and Nasopharyngeal Swabs : Towards Perspective COVID-19 Point-of-Care Diagnostics, *Int J Mol Sci*, 2023, **24**, 9706.

14 S. M. Mousavi, S. A. Hashemi, V. Rahmanian, M. Y. Kalashgrani, A. Gholami, N. Omidifar and W. H. Chiang, Highly Sensitive Flexible SERS-Based Sensing Platform for Detection of COVID-19, *Biosensors (Basel)*, 2022, **12**, 466.

15 V. Karunakaran, M. M. Joseph, I. Yadev, H. Sharma, K. Shamna, S. Saurav, R. P. Sreejith, V. Anand, R. Beegum, S. Regi David, T. Iype, K. L. Sarada Devi, A. Nizarudheen, M. S. Sharmad, R. Sharma, R. Mukhiya, E. Thouti, K. Yoosaf, J. Joseph, P. Sujatha Devi, S. Savithri, A. Agarwal, S. Singh and K. K. Maiti, A non-invasive ultrasensitive diagnostic approach for COVID-19 infection using salivary label-free SERS fingerprinting and artificial intelligence, *J Photochem Photobiol B*, 2022, **234**, 112545.

16 S. Srivastav, A. Dankov, M. Adanalic, R. Grzeschik, V. Tran, S. Pagel-Wieder, F. Gessler, I. Spreitzer, T. Scholz, B. Schnierle, O. E. Anastasiou, U. Dittmer and S. Schlücker, Rapid and Sensitive SERS-Based Lateral Flow Test for SARS-CoV2-Specific IgM/IgG Antibodies, *Anal Chem*, 2021, **93**, 12391–12399.

17 R. A. Halvorson and P. J. Vikesland, *Environ Sci Technol*, 2010, 44, 7749–7755.

18 X. Xu, S. Yang, Y. Wang and K. Qian, Nanomaterial-based sensors and strategies for heavy metal ion detection, *Green Analytical Chemistry*, , DOI:10.1016/j.greeac.2022.100020.

19 L. Mikac, I. Rigó, L. Himics, A. Tolić, M. Ivanda and M. Veres, Surface-enhanced Raman spectroscopy for the detection of microplastics, *Appl Surf Sci*, 2023, **608**, 155239.

20 E. Segal, E. Haleva and A. Salomon, Ultrasensitive Plasmonic Sensor for Detecting Sub-PPB Levels of Alachlor, *ACS Appl Nano Mater*, 2019, **2**, 1285–1293.

21 T. Xie, Z. Cao, Y. Li, Z. Li, F. L. Zhang, Y. Gu, C. Han, G. Yang and L. Qu, Highly sensitive SERS substrates with multi-hot spots for on-site detection of pesticide residues, *Food Chem*, 2022, **381**, 132208.

22 A. Jiao, X. Dong, H. Zhang, L. Xu, Y. Tian, X. Liu and M. Chen, Construction of pure worm-like AuAg nanochains for ultrasensitive SERS detection of pesticide residues on apple surfaces, *Spectrochim Acta A Mol Biomol Spectrosc*, 2019, **209**, 241–247.

23 S. Pang, T. Yang and L. He, Review of surface enhanced Raman spectroscopic (SERS) detection of synthetic chemical pesticides, *TrAC - Trends in Analytical Chemistry*, 2016, **85**, 73–82.

24 M. L. Xu, Y. Gao, X. X. Han and B. Zhao, Detection of Pesticide Residues in Food Using Surface-Enhanced Raman Spectroscopy: A Review, *J Agric Food Chem*, 2017, **65**, 6719–6726.

25 T. Wang, S. Wang, Z. Cheng, J. Wei, L. Yang, Z. Zhong, H. Hu, Y. Wang, B. Zhou and P. Li, Emerging core–shell nanostructures for surface-enhanced Raman scattering (SERS) detection of pesticide residues, *Chemical Engineering Journal*, 2021, **424**, 130323.

26 Y. Zhu, M. Li, D. Yu and L. Yang, A novel paper rag as 'D-SERS' substrate for detection of pesticide residues at various peels, *Talanta*, 2014, **128**, 117–124.

27 Y. Sun, W. Li, L. Zhao, F. Li, Y. Xie, W. Yao, W. Liu and Z. Lin, Simultaneous SERS detection of illegal food additives rhodamine B and basic orange II based on Au nanorod-incorporated melamine foam, *Food Chem*, 2021, **357**, 129741.

28 N. Peica, I. Pavel, S. Cîntă Pînzaru, V. K. Rastogi and W. Kiefer, Vibrational characterization of E102 food additive by Raman and surface-enhanced Raman spectroscopy and theoretical studies, *Journal of Raman Spectroscopy*, 2005, **36**, 657–666.

29 N. Peica, C. Lehene, N. Leopold, S. Schlücker and W. Kiefer, Monosodium glutamate in its anhydrous and monohydrate form: Differentiation by Raman spectroscopies and density functional calculations, *Spectrochim Acta A Mol Biomol Spectrosc*, 2007, **66**, 604–615.

30 X. Zheng, P. Guo, Y. Zhang, J. Xu, J. Sun and Y. Lei, An ultra sensitive and rapid SERS detection method based on vortex aggregation enhancement effect for anti-infective drug residues detection in water, *Anal Chim Acta*, 2022, **1235**, 340539.

31 M. Li and X. Zhang, Nanostructure-Based Surface-Enhanced Raman Spectroscopy Techniques for Pesticide and Veterinary Drug Residues Screening, *Bulletin of Environmental Contamination and Toxicology* , 2021, **107**, 194–205.

32 Z. Yang, C. Ma, J. Gu, Y. Wu, C. Zhu, L. Li, H. Gao, W. Yin, Z. Wang and G. Chen, Detection of melamine by using carboxyl-functionalized Ag-COF as a novel SERS substrate, *Food Chem*, 2023, **401**, 134078.

33 J. Cheng, P. Wang and X. O. Su, Surface-enhanced Raman spectroscopy for polychlorinated biphenyl detection: Recent developments and future prospects, *TrAC - Trends in Analytical Chemistry*, 2020, **125**, 15836.

34 J. Lin, O. U. Akakuru and A. Wu, Advances in surface-enhanced Raman scattering bioprobes for cancer imaging, *View*, 2021, **2**, 10–1002.

35 J. Lin, X. Ma, A. Li, O. U. Akakuru, C. Pan, M. He, C. Yao, W. Ren, Y. Li, D. Zhang, Y. Cao, T. Chen and A. Wu, Multiple valence states of Fe boosting SERS activity of Fe3O4 nanoparticles and enabling effective SERS-MRI bimodal cancer imaging, *Fundamental Research*, 2022, **10**, 2667–3258.

36 X. Huang, B. Sheng, H. Tian, Q. Chen, Y. Yang, B. Bui, J. Pi, H. Cai, S. Chen, J. Zhang, W. Chen, H. Zhou and P. Sun, Real-time SERS monitoring anticancer drug release along with SERS/MR imaging for pH-sensitive chemo-phototherapy, *Acta Pharm Sin B*, 2023, **13**, 1303–1317.

37 P. In, Surface Plasmon Properties of Hollow Auagalloyed Triangular Nanoboxes and its Ap-plications in SERS Imaging abd Potential Drug Delivery, *Progress In Electromagnetics Research*, 2012, **128**, 35–53.

38 Y. Wang, L. Polavarapu and L. M. Liz-Marzán, Reduced graphene oxide-supported gold nanostars for improved SERS sensing and drug delivery, *ACS Appl Mater Interfaces*, 2014, **6**, 21798–21805.

39 F. Tian, J. Conde, C. Bao, Y. Chen, J. Curtin and D. Cui, Gold nanostars for efficient in vitro and in vivo real-time SERS detection and drug delivery via plasmonic-tunable Raman/FTIR imaging, *Biomaterials*, 2016, **106**, 87–97.

40 F. Hu, Y. Zhang, G. Chen, C. Li and Q. Wang, Double-walled Au nanocage/SiO2 nanorattles: Integrating SERS imaging, drug delivery and photothermal therapy, *Small*, 2015, **11**, 985–993.

41 R. B. T.-P.-B. D. D. Vardanyan, Ed., in *Heterocyclic Drug Discovery*, Elsevier, 2017, pp. i–iii.

42 E. Vitaku, D. T. Smith and J. T. Njardarson, Analysis of the structural diversity, substitution patterns, and frequency of nitrogen heterocycles among U.S. FDA approved pharmaceuticals, *J Med Chem*, 2014, **57**, 10257–10274.

43 A. Schnabel, B. Athmer, K. Manke, F. Schumacher, F. Cotinguiba and T. Vogt, Identification and characterization of piperine synthase from black pepper, Piper nigrum L., *Commun Biol*, 2021, **4**, 1–10.

44 G. B. Neurath, M. Dünger, F. G. Pein, D. Ambrosius and O. Schreiber, Primary and secondary amines in the human environment, *Food Cosmet Toxicol*, 1977, **15**, 275–282.

45 U. S. v. Euler, The Occurrence and Determination of Piperidine in Human and Animal Urine1), *Acta Pharmacol Toxicol (Copenh)*, 1945, **1**, 29–59.

46 A. R. Tricker, B. Pfundstein, T. Kalble and R. Preussmann, Secondary amine precursors to nitrosamines in human saliva, gastric juice, blood, urine and faeces, *Carcinogenesis*, 1992, **13**, 563–568.

47 *Piperidine: Human health tier II assessment*, 2016.

48 S. Ameen, M. S. Akhtar, H. K. Seo and H. S. Shin, An electrochemical sensing platform based on hollow mesoporous ZnO nanoglobules modified glassy carbon electrode: Selective detection of piperidine chemical, *Chemical Engineering Journal*, 2015, **270**, 564–571.

49 R. Khan, U. Periyayya, G. C. Kim and I. H. Lee, Fabrication of ultra-sensitive piperidine chemical sensor with a direct

View Article Online
DOI: 10.1039/D3EN00821E

grown well-aligned ZnO nanorods on FTO substrate as a working electrode, *Solid State Sci*, 2019, **97**, 105986.

50 L. A. Sanchez, R. L. Birke and J. R. Lombardi, Surface-enhanced Raman scattering of piperidine. The effect of electrode potential on intensity, *Journal of Physical Chemistry*, 1984, **88**, 1762–1766.